pubs.acs.org/Biomac

Article

On the Conformation of Anionic Peptoids in the Gas Phase

Perrine Weber, Sébastien Hoyas, Émilie Halin, Olivier Coulembier, Julien De Winter, Jérôme Cornil,* and Pascal Gerbaux*

Cite This: https://doi.org/10.1021/acs.biomac.1c01442

Read Online

ACCESS | Metrics & More | Article Recommendations | Supporting Information

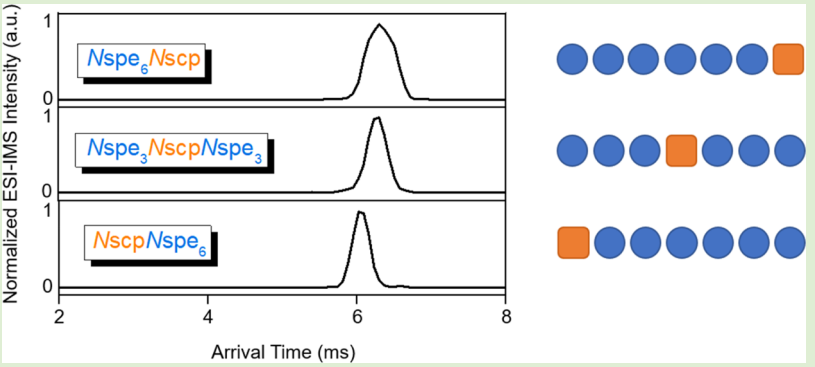

ABSTRACT: Although *N*-(*S*)-phenylethyl peptoids are known to adopt helical structures in solutions, the corresponding positively charged ions lose their helical structure during the transfer from the solution to the gas phase due to the so-called charge solvation effect. We, here, considered negatively charged peptoids to investigate by ion mobility spectrometry−mass spectrometry whether the structural changes described in the positive ionization mode can be circumvented in the negative mode by a fine-tuning of the peptoid sequence, that is, by positioning the negative charge at the positive side of the helical peptoid macrodipole. *N*-(*S*)-(1-carboxy-2-phenylethyl) (*Nscp*) and *N*-(*S*)-phenylethyl (*Nspe*) were selected as the negative charge carrier and as the helix inductor, respectively. We, here, report the results of a joint theoretical and experimental study demonstrating that the structures adopted by the *Nspe*$_n$*Nscp* anions remain compactly folded in the gas phase for chains containing up to 10 residues, whereas no evidence of the presence of a helical structure was obtained, even if, for selected sequences and lengths, different gas phase conformations are detected.

INTRODUCTION

Since the introduction of electrospray ionization (ESI), numerous research groups endeavored to investigate the gas phase conformations of biological molecules, such as proteins and nucleic acids, using mass spectrometry (MS) methods.[1−4] These studies benefit from the fact that the solution phase structures are preserved when using native MS methods and mostly concentrate on large-molecular-weight compounds, such as large proteins or protein assemblies.[3,5,6] On the other hand, other research groups focus their interest on the determination of the intrinsic molecular interactions responsible for the conformations adopted by ionized molecules in the gas phase, often using small model systems such as small peptides.[7−10] Ion mobility spectrometry (IMS) coupled to mass spectrometry (IMS−MS) is nowadays increasingly used to afford structural data on gas phase ions, with a special interest paid to proteins, peptides, nucleic acids, and synthetic polymers.[11−15] Interestingly, secondary structures *in vacuo*[16−18] can be established by confronting MS information to computational chemistry data.[8,19,20] It is now largely demonstrated that the structure of (macro)molecules may be strongly modified upon ionization and gas phase transfer; in particular, flexible molecules typically fold around the charge site upon solvent molecule evaporation.[8,21−24] This effect, known as the "charge solvation effect", questions the relevance of MS for the structural analysis of macromolecules, especially to deduce condensed phase structures based on gas phase investigations.[8,21−24]

Poly-*N*-substituted glycines or peptoids represent an emergent class of synthetic peptidomimetic polymers (Scheme 1).[25] The main difference with peptides is the side chain position on the backbone, appended to the amide nitrogen atom rather than to the α-carbon.[25]

Various efficient synthetic protocols developed over the years and the wide diversity of commercially available amines

Received: November 4, 2021
Revised: December 17, 2021

Scheme 1. General Primary Structure of Peptoids Represented from N to C Extremities[a]

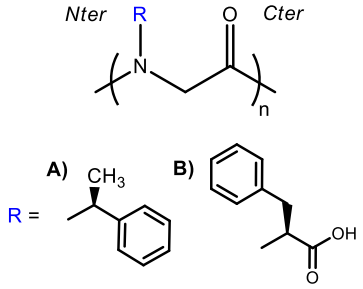

[a]The side chains R studied are (A) (*S*)-*N*-(1-phenylethyl) (*N*spe) and (B) (*S*)-*N*-(1-carboxy-2-phenylethyl) (*N*scp).

allow preparing peptoids with specific designs adapted to diverse applications (therapeutic, catalysis, etc.).[26−30] This together with their wide structural diversity[31−36] and their high resistance to protease[37] as well as to temperature or solvent changes[38] clearly represent strong assets over peptides for targeted—including *in vivo*—applications. Depending on their sequence, peptoids may adopt different stabilized secondary structures, that is, helix,[31] threaded-loop, or ribbon,[32,34] in solutions and in the solid state.[31,32,34] Helical conformations are the most studied and exploited foldamer structures in the biomedical field[39,40] and in material science.[29,40] Peptoid helices in solutions are stabilized when the side chain is bulky and chiral, as promoted by the (*S*)-*N*-(1-phenylethyl) (*N*spe) side chain (Scheme 1).[41] Structural studies on such helices are generally performed using circular dichroism spectroscopy, revealing a signature analogous to the peptide α-helix, and by nuclear magnetic resonance spectroscopy.[41,42] Recently, using the combination of IMS−MS and molecular dynamics (MD) simulations, we demonstrated that helical peptoids based on *N*spe units formed in solutions do not retain their secondary structure when transferred in the gas phase and rather adopt loop-like structures caused by the charge solvation effect.[23] Actually, the secondary interactions stabilizing helices in solutions, that is, steric hindrance and electrostatic effects,[41] are not sufficient to compensate the charge solvation effect. MD simulations revealed that strong charge/dipole interactions between the C═O groups and the proton (ammonium group) induce the folding of the peptoid ions around the charge and the loss of the extended helical structure. In a second study, we introduced additional non-covalent interactions through H-bond donor groups (carboxylic acid moieties) carried by the pending side chains.[43] Using the IMS−MS/MD approach, we detected helices in the gas phase cemented by the formation of an intra-residue H-bond network associating the hydrogen atom from the side chain carboxylic acid to the oxygen atom of the amide inside the same residue. We further demonstrated that the obtention of stable peptoid helices in the gas phase is conditioned by different factors: (i) the possibility to create a H-bond network; (ii) the presence of a sufficient amount of residues to energetically counterbalance the charge induced folding; and (iii) the presence of bulky side chains to rigidify the backbone (generate a high degree of steric hindrance).[43]

In the present study, we want to assess whether helical peptoid ions can be stabilized in the gas phase using the "macrodipole approach",[44] successfully employed for the detection of helical peptides in the gas phase. Although helical in solutions, protonated poly(alanine) ions with up to 20 residues do not retain their shape in a vacuum-like environment since the charge destabilizes the helical conformation (Scheme 2).[8] However, the addition of a single lysine residue at the C terminus of acetylated poly(alanine)s results in the formation of very stable lysine-protonated poly(alanine) helices, whose positive charge created by the addition of the proton is locally stabilized by the surrounding amides as well as by the negative end of the poly(alanine) helix macrodipole (Scheme 2).[45] Such a favorable charge/macrodipole interaction thus appears beneficial to preserve/develop helices in the gas phase. Armand *et al.* reported that the macrodipole of helical *N*spe peptoids is opposite to that of the poly(alanine) helix with the negative end located at the N terminus side (Scheme 3).[42] In this case, as described above, protonated *N*spe peptoids do not preserve their helical structure in the gas phase.[23]

Scheme 2. Helical Structures of (A) Poly(alanine)s and (C) Acetylated Poly(alanine)s with a C Terminal Lysine Are Characterized by a Macrodipole[a]

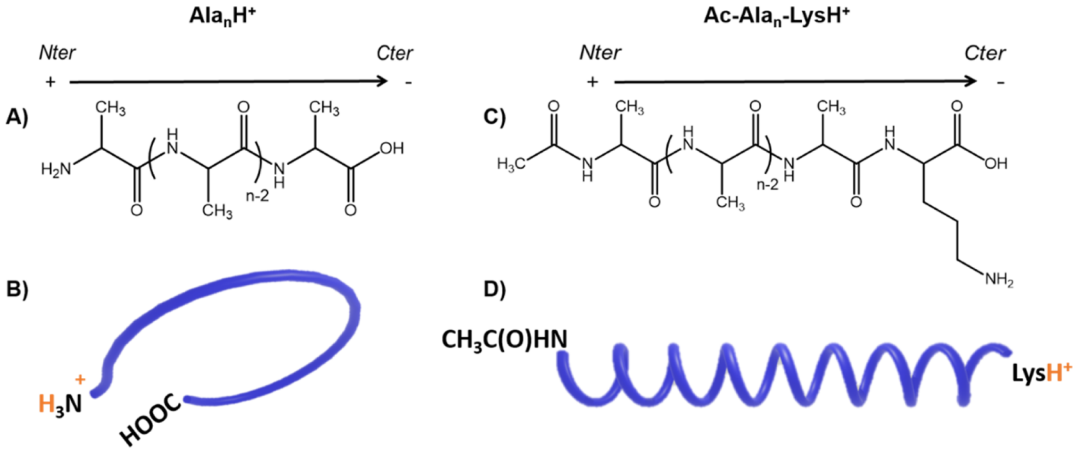

[a]Upon transfer in the gas phase, protonated Ala$_n$ (B) does not retain the helical structure, while protonated Ac-Ala$_n$-Lys (D) is detected as a stable helice due to the protonation at the Cter side of the peptide, that is, the negative side of the helix macrodipole.[7] The modeled structures are adapted from ref 7.

https://doi.org/10.1021/acs.biomac.1c01442
Biomacromolecules XXXX, XXX, XXX−XXX

Scheme 3. Molecular Structures of (A) Protonated *N*-(*S*)-Phenylethyl Peptoid ($Nspe_nH^+$) and (B) Deprotonated *N*-(*S*)-Phenylethyl-*N*-(*S*)-(1-carboxy-2-phenylethyl) Peptoid ($Nspe_{n-1}Nscp^-$)

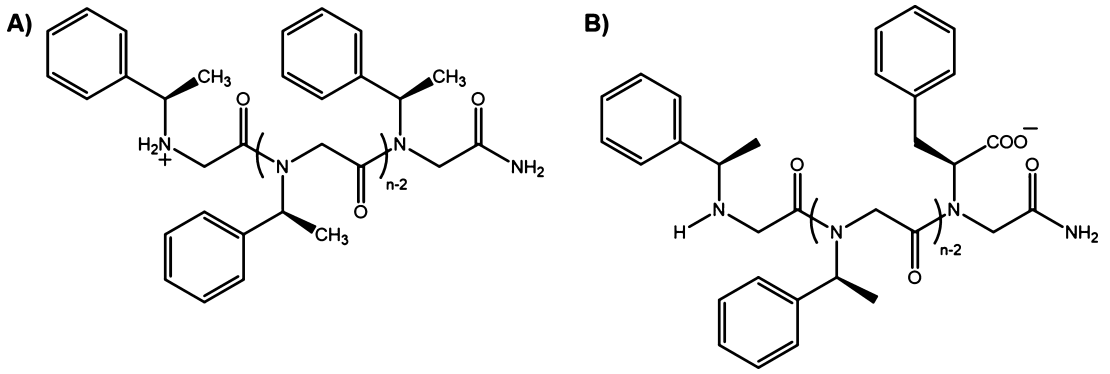

Figure 1. Peptoid dihedral angles and their nomenclature: conversion between dihedral angle values and letter codes for attributing the peptoid conformations.

We would like to establish here whether anionic peptoids in the gas phase may be detected as extended helices by using the IMS−MS/MD combination. The last residue at the C terminus side of these peptoids carries a carboxylic acid that is deprotonated, providing an interaction with the positive end of the helical peptoid macrodipole. To achieve that goal, we designed hetero-peptoid sequences based on *N*spe residues and a single *N*scp (*S*)-*N*-(1-carboxy-2-phenylethyl) residue. The *N*scp carries the carboxylic acid moiety that is easily deprotonated under negative ionization mode in MS analyses (Scheme 3). In a first approach, the *N*scp residue will be located at the C terminus and the influence of the peptoid length monitored, while in a second approach, we will vary the position of the *N*scp in the backbone.

MATERIALS AND METHODS

Nomenclature. The conformational landscape of peptoids is mostly described by their backbone dihedral angles, that is, ω, φ, and ψ, which are shown in Figure 1.[46] Secondary structures are defined by particular combinations of these three dihedral angles. The typical example is a perfect right-handed helix, characterized by a periodic repetition of the pattern ($\omega \sim 0°$, $\varphi \sim -80°$, $\psi \sim 180°$).[42] Spencer *et al.* showed that the individual backbone dihedral angles of most peptoids systematically have the same range of values.[46] Therefore, to simplify the attribution of the secondary structures, they developed a nomenclature that associates a letter to a particular range of values for a given dihedral angle (Figure 1). For example, they described ψ by the capital letter *Z* (about 180°), φ by *R* (left-handed) or *S* (right-handed), and ω by c (cis) or t (trans). Using this nomenclature, a residue included within a right-handed helix is now described as "Z_{Sc}", where the first letter is related to the ψ dihedral angle, while the second and third are related to the φ and ω dihedral angles, respectively.[29] However, this nomenclature is very limitative and does not allow the description of dihedral angles whose values are outside the defined range, in particular when $\psi \sim 0°$. Therefore, we introduce here an additional letter to characterize this dihedral angle, namely Θ, when ψ is close to 0°.

In the present study, we observed that the vast majority of the peptoid residues are either in a "Z_{Rc}" or a "Z_{Sc}" conformation. Therefore, we decided to further simplify the notation by attributing a single letter to the three-letter code, which is especially useful for the readability of long peptoid sequences. We denominated the "Z_{Rc}" as "*G*" and "Z_{Sc}" as "*D*". If a residue is not in such a conformation, the complete letter code of this residue will be written instead.

Computational Chemistry. Calculations were performed at the density functional theory (DFT) level of theory using the CAM-B3LYP functional and a 6-31G** double zeta basis set, as implemented in the Gaussian 16 (A03 revision) software.[47] Empirical Grimme's term D3 correction was used to improve the description of the dispersion interactions, and the functional is abbreviated as CAM-B3LYP-D3 throughout the article.[48] Each molecular structure was fully optimized, and minima were confirmed through vibrational analysis. We generated each starting geometry based on dihedral angle values commonly reported in the literature.[46] Since the number of possible conformers rapidly grows with size, we only considered all conformers for peptoid chain lengths ranging from 1 to 4 (see the text for more details). For longer chains, we created input geometries based on the most stable conformers obtained for the shorter chains. Each optimized geometry was then subjected to collision cross section (CCS, $^{TM}\Omega_{He}$) calculations using the Collidoscope software using the "trajectory method" (TM) with helium as the collision gas.[49]

Peptoid Synthesis. All reactants and solvents were commercially obtained (VWR Chemicals) and are used without any supplementary purification. The synthesis of $Nspe_nNscp$ peptoids was performed using the solid-phase reaction protocol reported by Zuckermann and co-workers consisting of successive acylation and nucleophilic substitution steps on the Rink amide resin: all details are described elsewhere.[25] The amines used during the nucleophilic substitution

https://doi.org/10.1021/acs.biomac.1c01442
Biomacromolecules XXXX, XXX, XXX−XXX

were (*S*)-phenylethylamine and L-phenylalanine previously esterified to protect carboxyl groups during the peptoid synthesis with the following procedure: at 0 °C, thionyl chloride (11 mL, 0.15 mol) was slowly added to methanol (150 mL). Phenylalanine was added at room temperature and stirred for 48 h. After the solvent evaporation, the esterified phenylalanine was purified by washing with a saturated solution of Na_2CO_3, extracted with dichloromethane and concentrated *in vacuo*. After the synthesis of the *N*spe$_{2-9}$*N*scp sequences, the carboxyl groups were deprotected by hydrolysis with NaOH 5 M (3 mL) and methanol (4 mL) at 55 °C for 5 h. *N*spe$_{2-9}$*N*scp peptoids were prepared without further purification since they were only analyzed by MS. The characterization was achieved with the determination of the mass-to-charge ratio of the corresponding ions $[M + H]^+$ and with collision-induced dissociation experiments (Table S1).

Ion Mobility Experiments. Ion mobility measurements were performed using a Synapt G2-*Si* (Waters, UK) mass spectrometer equipped with an ESI source and a traveling wave ion mobility cell operated in N_2 as the drift gas. The IMS parameters and the sample preparation are described in the Supporting Information. In TWIMS experiments, a calibration using deprotonated polyalanines[50] was required to convert drift times measured in nitrogen into CCSs in helium ($^{TW}\Omega_{N2\rightarrow He}$).[51] The CCSs Ω were abbreviated by using the current notation;[18] $^{TW}\Omega_{N2\rightarrow He}$ represent experimental CCSs, while $^{TM}\Omega_{He}$ correspond to theoretical CCSs.

RESULTS AND DISCUSSION

Figure 2 presents hypothetical ideal helix structures (viewed along the helix axis from the C terminus at the bottom) for

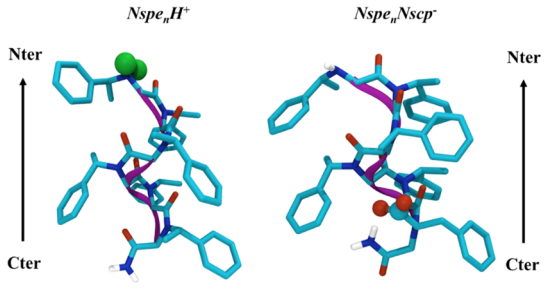

Figure 2. Hypothetical ideal helix structures for *N*spe$_n$H$^+$ and *N*spe$_n$*N*scp$^-$ peptoid ions. The hydrogen atoms highlighted as green beads correspond to the $-NH_2^+$ ammonium moiety in the *N*spe$_n$H$^+$ peptoid ion, whereas the oxygen atoms of the carboxylate group are represented as red beads in the *N*spe$_n$*N*scp$^-$ peptoid ion. The structures are built using the dihedral angles determined by Armand *et al.*[42] and optimized at the CAM-B3LYP-D3 level of theory.

*N*spe$_n$H$^+$ and *N*spe$_n$*N*scp$^-$ peptoids. These helices were obtained by DFT optimization of input structures generated using the backbone dihedral angles (ω, φ, and ψ) defined by Armand *et al.*[42] for perfect right-handed helical structures. The helical backbones are highlighted by the purple ribbons. The most relevant difference between both hypothetical structures is the orientation of the C=O dipoles whose negative (δ−) sides are all pointing toward the ammonium group in the *N*spe$_n$H$^+$ peptoid and away from the carboxylate group in the *N*spe$_n$*N*scp$^-$ peptoid. We already noted that, in the case of the positively charged ions, such an arrangement does not prevent the peptoid backbone from collapsing around the ammonium group.[23] In the following paragraphs, we would like to test whether with tailor-made *N*spe$_n$*N*scp$^-$ candidates in the negative ionization mode, extended peptoids can be detected in the gas phase using IMS−MS.

In a bottom-up approach, we decided to study the gas phase structures of the *N*spe$_n$*N*scp peptoid anions with a growing chain (n = 2−9), both experimentally using IMS−MS and theoretically using DFT calculations. Using this combined approach, we assessed the impact of the charged site on the gas phase structure of the peptoid anions, namely, the carboxylate group ($RCOO^-$) created upon ESI at the C terminus side of the peptoids.

Before studying complete peptoid sequences, we first considered theoretically the shortest possible structure that is constituted by a single *N*scp side chain with an acetyl group positioned on the nitrogen amine atom, that is, Ac*N*scp$_1$, to mimic the basic motif on which the molecular backbone will grow. As recently pointed out by Spencer *et al.*, peptoids may adopt different backbone dihedral angle combinations.[46] The amide bond can be in *cis* or *trans* conformation, while the φ dihedral angle can be positive or negative (±~90°) and the ψ dihedral angle around 0° or 180°. Every residue is thus characterized by three dihedral angles that can adopt two values each, leading to $2 \times 2 \times 2 = 2^3$ possible combinations for a single residue or more precisely for each amide bond. In the present case, Ac*N*scp$_1$ would then adopt up to eight different conformations. We can generalize for any chain size the total number of possible combinations as $(2^3)^{\#\text{amide bond}}$.

The four most stable conformations obtained using DFT calculations are presented in Figure 3. One of the key

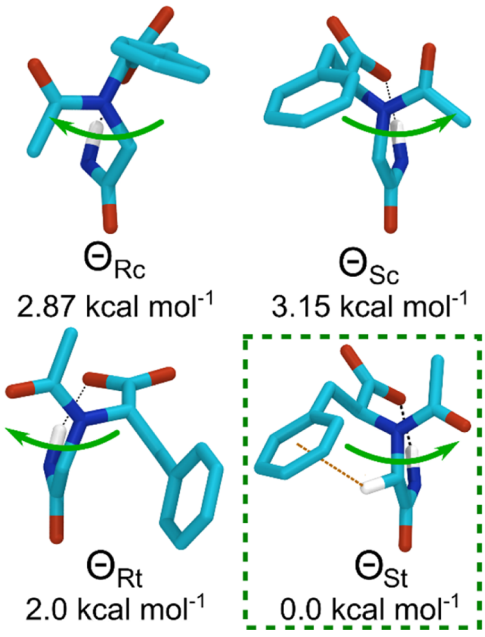

Figure 3. Four conformers of Ac*N*scp$_1$ denoted by their nomenclature codes. Hydrogen atoms are omitted for clarity, except those involved in the stabilizing interactions. Hydrogen bonds and CH−π interactions are denoted by black dotted lines. Green arrows indicate the "rotational sense" of each conformer. The relative energies were obtained using DFT calculations at the CAM-B3LYP-D3 level of theory.

observations when considering these structures is that the ψ dihedral angle systematically shifts to ~0°, inducing Θ conformations (see Figure 1), whereas this dihedral angle is around 180° for most of the peptoid residues (*Z* conformations).[46] This is due to the presence of the carboxylate moiety that is involved in a strong hydrogen

https://doi.org/10.1021/acs.biomac.1c01442
Biomacromolecules XXXX, XXX, XXX−XXX

Scheme 4. Primary Sequence of the Non-acetylated Peptoid Trimer *N*spe$_2$*N*scp and Its Associated Backbone Dihedral Angles

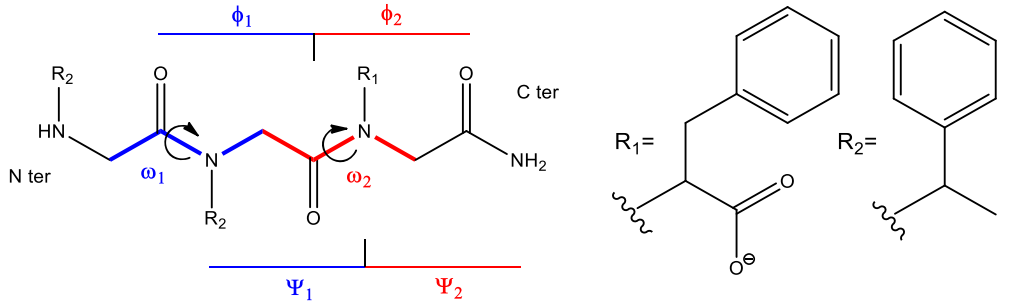

Scheme 5. Trans or Cis Conformations of the Amide Bond of the *N*spe Residue Directly Attached on the C Terminus *N*scp Residue[a]

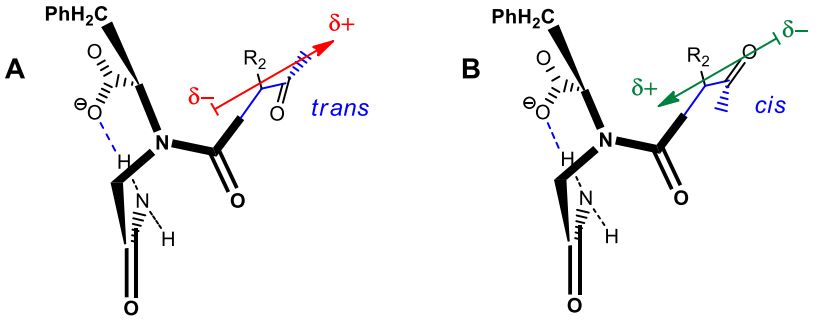

[a]In the trans/cis conformation (A/B), the negative ($\delta-$)/positive side ($\delta+$) of the amide dipole (in red/green) is pointing in the direction of the carboxylate group, thus favoring the B form.

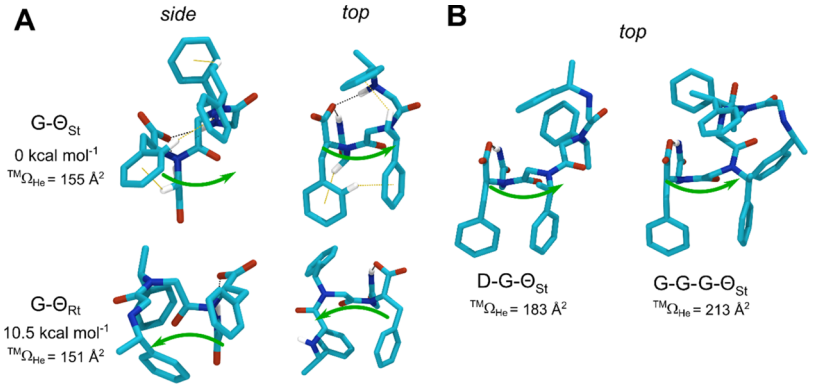

Figure 4. (A) Most stable *N*spe$_2$*N*scp conformers. Hydrogen atoms are omitted for clarity, except those involved in stabilizing interactions. Hydrogen bonds and CH−π interactions are denoted by black dotted lines and orange dotted lines, respectively. Green arrows indicate the "rotation sense" of each conformer. (B) Most stable *N*spe$_3$*N*scp (left) and *N*spe$_4$*N*scp (right) conformers. The relative energies were obtained using DFT calculations at the CAM-B3LYP-D3 level of theory. $^{TM}\Omega_{He}$ correspond to the theoretical CCSs (see the Materials and Methods for computational details).

bond with an amide hydrogen atom (with a distance of around 1.75 Å between the hydrogen and the acceptor and an angle of 170° in the donor−hydrogen−acceptor triad), as highlighted in Figure 3.

Also, depending on the sign of φ, the structures present their growing chain "turning" either left (Θ_{St}) or right (Θ_{Rt}) when the C terminus amide is placed vertically (see the green arrows in Figure 3). A positive φ will trigger a rotation to the left, while a negative φ will induce a rotation to the right. The same observation is valid for both *cis* and *trans* amide conformers. Among these conformers, Ac*N*scp$_1$-Θ_{St} is the most stable, by about 2 kcal/mol (Figure 3). The main stabilizing factor is, besides the hydrogen bond common to all conformers, a CH−π interaction between the phenyl ring and the amide methylene (Figure 3). This first residue is therefore most likely locked into the Θ_{St} conformation.

When considering a slightly longer peptoid by adding 2 *N*spe residues on the N terminus side (*N*spe$_2$*N*scp, Scheme 4), the number of possible conformations rapidly increases. Indeed, there are 2 amide bonds, so that the total number of possible conformations is $(2^3)^2 = 64$.

Fortunately, we can narrow down this number. Indeed, since the ψ dihedral angle is generally around 180°, except for the *N*scp residue (which is rather at ∼ 0° according to our calculations on Ac*N*scp$_1$), ψ only takes one of the two values, generating a reduced number of conformers: $(2^2)^2 = 16$. Moreover, if we add an *N*spe residue at the N terminus on the Ac*N*scp$_1$, its amide bond can adopt either a *cis* ($\omega \sim 0°$) or a

https://doi.org/10.1021/acs.biomac.1c01442
Biomacromolecules XXXX, XXX, XXX−XXX

trans ($\omega \sim 180°$) conformation. However, a trans conformation is unlikely because of the non-favorable orientation of the amide dipole toward the carboxylate (Scheme 5). All together, these considerations lead to the conclusion that the φ dihedral angle will dictate the number of conformers available, which is thus reduced to $(2^1)^2 = 4$.

The most stable among the four possible conformers (Figure S1) is characterized by the sequence $G{-}\Theta_{St}$ (in other terms, $Z_{Rc}{-}\Theta_{St}$). In this conformation (Figure 4), the last *N*scp residue has the same geometry as in the model peptoid Ac*N*scp$_1$, with a hydrogen bond still present between the carboxylate and the amide hydrogen as well as with the CH$-\pi$ interaction between the methylene group and the phenyl ring, which appears to lock the C terminus in that geometry. Compared to the other conformers (Figure S1), $G{-}\Theta_{St}$ is even more stabilized due to the presence of additional CH$-\pi$ interactions between the side chains but also due to a hydrogen bond between the amine at the N terminus and the carboxylate (Figure 4A). The chirality of the *N*scp side chain dictates locally in which sense the chain will "turn" to create more favorable interactions. Indeed, as shown in Figure 4A, if we consider $G{-}\Theta_{St}$ and $G{-}\Theta_{Rt}$, the CH$-\pi$ interaction (between the *N*scp phenyl and the *N*spe phenyl) cannot be formed in the $G{-}\Theta_{Rt}$ geometry, making the $G{-}\Theta_{Rt}$ geometry significantly less stable (10.5 kcal mol^{-1}) than the $G{-}\Theta_{St}$ geometry. Interestingly, *N*spe$_3$*N*scp and *N*spe$_4$*N*scp have the same starting motif at the C terminus extremity as *N*spe$_2$*N*scp, that is, $G{-}\Theta_{St}$ (Figure 4B). This conformation is actually locked due to the hydrogen bond between the carboxylate and the terminal amide and the favorable interactions between the aromatic side chains. The chirality of the last residue at the C terminus thus appears to dictate the nature of the new secondary interactions between the side chains in these systems.

However, this local influence of the chirality vanishes with increasing chain length. Let us consider *N*spe$_5$*N*scp that has 2^5 possible conformers (32). Given the computational cost of DFT calculations for such large systems, we simulated only 16 of them based on the structural data obtained with shorter oligomers. Among these, we obtained two very stable conformers presenting different dihedral angle combinations, namely, $D{-}G{-}D{-}G{-}\Theta_{St}$ and $D{-}G{-}D{-}G{-}\Theta_{Rt}$ (Figure 5).

One striking difference between these two conformations concerns the *N*scp residue, whose φ dihedral angle is either positive (Θ_{Rt}) or negative (Θ_{St}), defining the rotation sense of the growing chain. As seen in Figure 5, both structures "turn" either right or left depending on the conformation of the C terminus *N*scp residue. However, the energy gained at the C terminus by the local favorable interactions in the Θ_{St} geometry (mostly CH$-\pi$) is not sufficient to dominate the energy stabilization provided further along the chain in the Θ_{Rt} geometry. Unfortunately, the computed CCSs ($^{TM}\Omega_{He}$) are identical, around 235 Å^2, preventing any separation by IMS–MS. When examining the corresponding IMS experimental data presented in Figure 6, we detected a single signal for the deprotonated *N*spe$_5$*N*scp peptoid with $^{TW}\Omega_{N2\rightarrow He}$ measured at 240 Å^2, nicely matching the theoretical CCS value ($^{TM}\Omega_{He}$).

From *N*spe$_6$*N*scp, see Figure 6, different conformations start to be separated upon IMS–MS, pointing to the presence of non-interconverting gas phase structures.[52,53] As a striking example, two nicely resolved signals are detected for the deprotonated *N*spe$_7$*N*scp with $^{TW}\Omega_{N2\rightarrow He}$ determined at 280 and 291 Å^2. Even if the observation of less compact/more extended ion structures from *N*spe$_6$*N*scp is established, the presence of a (quasi)helical structure remains elusive.

Monitoring the CCS evolution of polymer ions all along the molecular mass distribution, that is, plotting the CCS as a

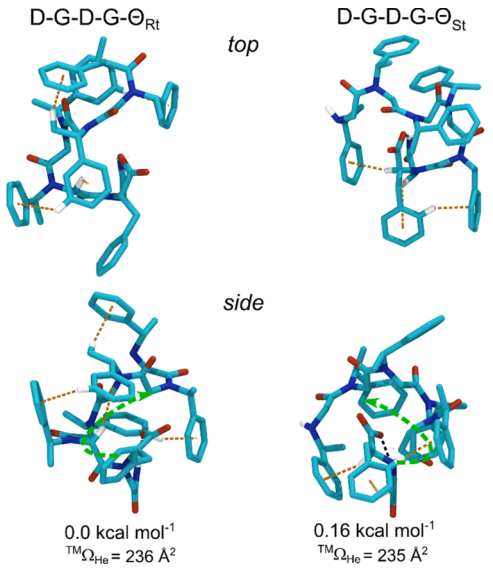

Figure 5. Most stable *N*spe$_5$*N*scp conformers. Hydrogen atoms are omitted for clarity, except those involved in stabilizing interactions. Hydrogen bonds and CH$-\pi$ interactions are denoted by black dotted lines and orange dotted lines, respectively. Green arrows indicate the "rotation sense" of each conformer. The relative energies were obtained using DFT calculations at the CAM-B3LYP-D3 level of theory.

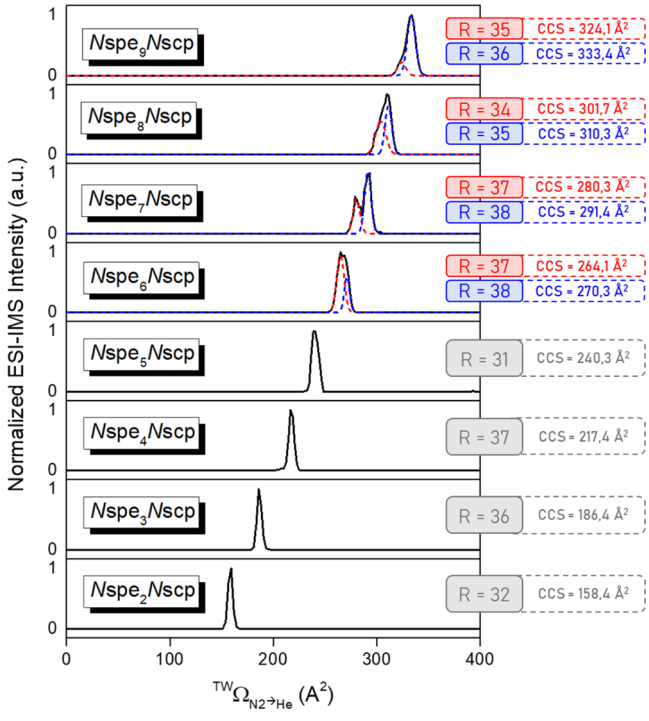

Figure 6. IMS analysis of deprotonated *N*spe$_n$*N*scp (n = 2–9) peptoids: CCS distributions ($^{TW}\Omega_{N2\rightarrow He}$) and CCS resolution ($R$ = CCS/ΔCCS$^{50\%}$). The deconvolution of the CCS signals for the *N*spe$_n$*N*scp with $n > 6$ reveals the presence of several differentiable structures. CCS resolutions have been determined on the deconvoluted signals.

https://doi.org/10.1021/acs.biomac.1c01442
Biomacromolecules XXXX, XXX, XXX–XXX

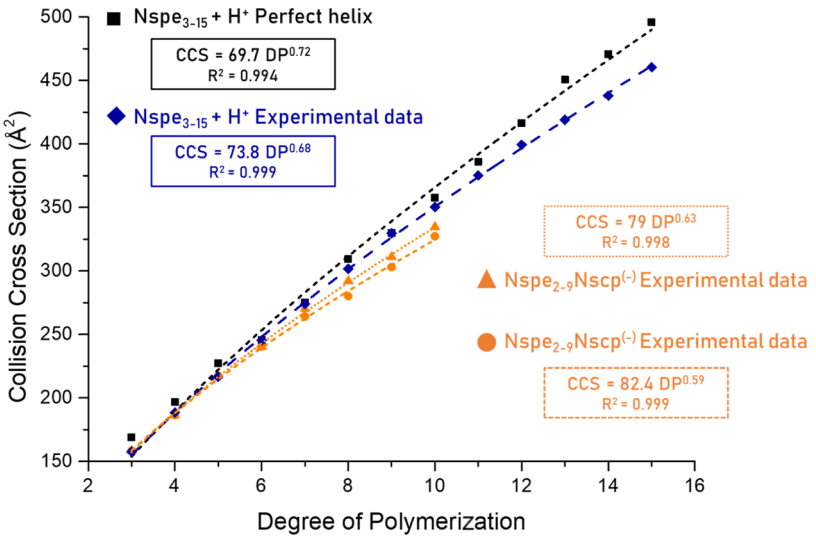

Figure 7. Experimental and theoretical CCSs of *N*spe ($[M + H]^+$) and *N*spe*N*scp ($[M - H]^-$) peptoid ions. Comparison of the size evolution of the theoretical experimental $^{TM}\Omega_{He}$ (black squares) for hypothetical *N*spe peptoid helices and the experimental $^{TW}\Omega_{N2\rightarrow He}$ for protonated *N*spe (blue diamonds) and for both distributions of deprotonated *N*spe*N*scp (orange triangles and circles). The theoretical/experimental data are fitted by the expression CCS = $A{\cdot}DP^B$. Note that for *N*spe$_n$*N*scp, DP = n +1.

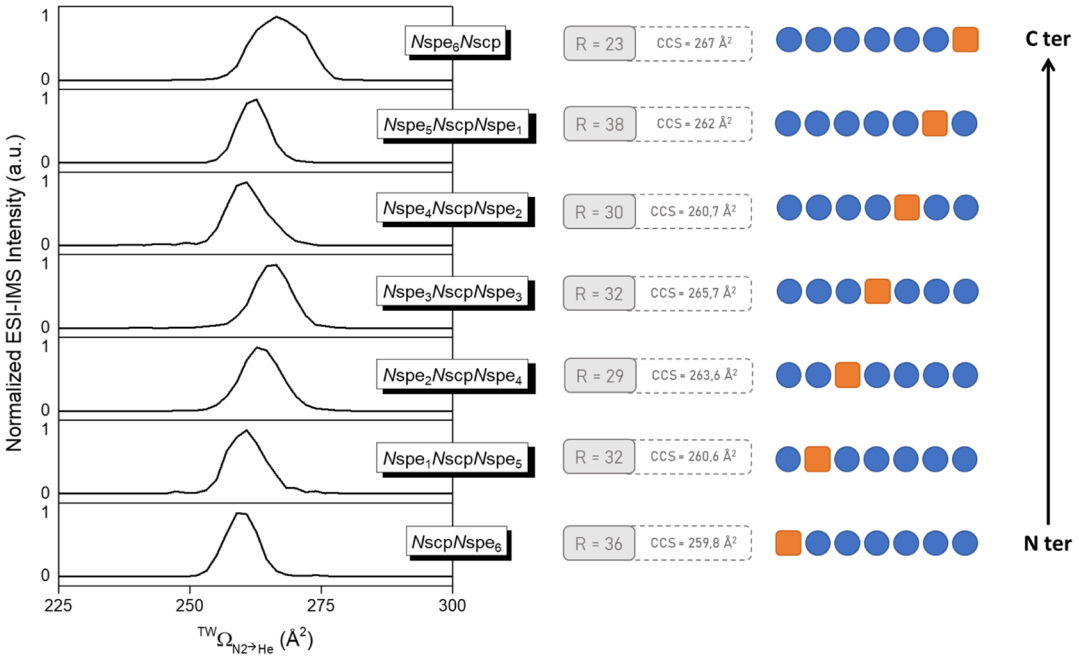

Figure 8. IMS analysis of deprotonated *N*spe$_n$*N*scp*N*spe$_m$ ($n + m = 6$) peptoids: CCS distributions ($^{TW}\Omega_{N2\rightarrow He}$) and CCS resolution ($R$ = CCS/$\Delta CCS^{50\%}$) of the different regioisomeric ions. The most striking observation is the significant loss of resolution for *N*spe$_6$*N*scp ions demonstrating the presence of different non-interconverting structures.

function of the degree of polymerization (or of the mass), is often proposed as a way to derive the structural (and physicochemical) properties of polymer ions.[51,52,54−56] This approach is based on the seminal study conducted by Ruotolo *et al.* that demonstrates that the CCS evolution with regard to the molecular mass of globular (protein) ions can be fitted with the following equation: CCS = $A{\cdot}DP^B$, where A and B are fitting parameters.[51] For globular ions that are assumed to be spherical objects, the B parameter is determined to be 2/3, as supported using a geometrical model.[23,51,57] We recently demonstrated using molecular modeling on peptoid ions that B critically depends on the mass range of data available for the fitting procedure for non-globular ions.[23] However, it is generally considered that a B parameter >2/3 indicates the presence of extended structures, such as helices for which B = 1 is geometrically expected for infinite helical structures.[23] In Figure 7, we compare the trend lines obtained for the *N*spe$_n$*N*scp ion series with the data previously reported on protonated *N*spe.[23] We immediately noticed that, for a given DP (for *N*spe$_n$*N*scp, DP = n + 1), the deprotonated *N*spe$_n$*N*scp molecules are always more compact, that is, characterized by smaller CCS, than the corresponding $[N\text{spe} + H]^+$ ions that were demonstrated to adopt loop-like structures in a precedent study.[23] Also, when fitting separately the two ion families

https://doi.org/10.1021/acs.biomac.1c01442
Biomacromolecules XXXX, XXX, XXX−XXX

detected for the deprotonated $Nspe_nNscp$ peptoids, we determined two different B parameters, that is, B = 0.59 (orange circles) and B = 0.63 (orange triangles); these values further indicate that even the less compact ion structures cannot be considered as helical or extended structures in the gas phase. In other words, the *N*scp unit located at the C terminus cannot help to stabilize any helical structure in the gas phase despite the predicted macrodipole/charge attractive interaction (Figure 1).

Finally, the position of the negatively charged *N*scp residue is found to slightly influence the CCS of the corresponding ions, as revealed by the data in Figure 8. Indeed, when displacing the *N*scp residue from the C terminus to the N terminus position of the seven-residue peptoids ($Nspe_6Nscp$), we observe that the $^{TW}\Omega_{N2\rightarrow He}$ value is marginally affected. However, a striking difference is the presence of a large signal only for the $Nspe_6Nscp$ anions, that is, with the *N*scp residue at the C terminus of the peptoid sequence. This is clearly detected by the loss of resolution ($R \sim 20$ compared to the instrumental resolution of ~ 40), indicating the presence of multiple ion structures (see also Figure 6). It is rather interesting to observe that peptoid oligomers with the negative-charged *N*-substituent at the N terminus ($NscpNspe_6$) exhibit a much narrower ion mobility signal than that with the charged group at the C terminus ($Nspe_6Nscp$), which suggests the presence of a more uniform conformation set (or a single ion conformation) for the former. We suspect that a strong hydrogen bond between the Nter carboxylate group and the Cter amide function strengthens the loop conformation of the $NscpNspe_6$ ions, limiting hereby the conformational freedom. For the Cter case, the aforementioned local H-bond does not significantly reduce the conformational space explored by the growing chain(s), inducing a broadening of the CCS distribution.

Anyway, the absence of the most extended structure for all other regioisomers points to the crucial structuring role played by the *N*scp residue when positioned at the C terminus, as exemplified by our model $AcNscp_1$ system presented in Figure 3.

CONCLUSIONS

Over the past 20 years, peptoids have been extensively studied for their ability to adopt helices in solutions.[31,41] Nevertheless, the secondary structures in solutions are strongly dependent on the temperature and on the nature of the solvent.[31] Mass spectrometry together with IMS is a promising structural analysis method allowing to sample gas phase ions with limited conformational freedom.[16,18] However, as reported in previous studies related to positively charged peptoids,[23] charge solvation, that is, say charge stabilization upon folding, is responsible for the loss of the helical structure of *N*-(*S*)-phenylethyl peptoids during the transfer from a solution to a gas phase. We here considered negatively charged peptoids to investigate whether the structural changes produced by positive charges can be avoided by a fine-tuning of the peptoid sequence, that is, by changing the nature of the charge and positioning the negative charge at the positive side of the helical peptoid macrodipole. *N*-(*S*)-(1-carboxy-2-phenylethyl) (*N*scp) was selected as the negative charge carrier and *N*-(*S*)-phenylethyl (*N*spe) as the helical structure inductor. The joint theoretical and experimental study demonstrates that the structures adopted by the $Nspe_nNscp$ anions remain compactly folded in the gas phase for chains containing up to 10 residues and no evidence of the presence of a helical structure is obtained. However, the presence of differentiable stable structures was detected when the chain length increases though only when the negatively charged *N*scp residue is positioned at the C terminus. Our DFT calculations reveal that the negatively charged *N*scp residue at the C terminus predominantly adopts a Θ_{St} conformation stabilized by the presence of an H bond between the carboxylate group and the C terminus amide function and of a CH−π interaction between the phenyl ring and the amide methylene. For short sequences, such as $Nspe_{2-4}Nscp$, this conformation governs the structuration of the growing *N*spe chains, as revealed when analyzing regioisomeric peptoids. Nonetheless, the local influence of the *N*scp side chain chirality vanishes with increasing chain length, resulting experimentally in an enlargement or a bimodal distribution of the arrival time distribution for the $Nspe_{5-9}Nscp$ systems.

ASSOCIATED CONTENT

Supporting Information

The Supporting Information is available free of charge at https://pubs.acs.org/doi/10.1021/acs.biomac.1c01442.

Further details about peptoid synthesis and characterization, IMS protocols, and DFT complementary analyses, including *XYZ* coordinates of the $Nspe_nNscp$ conformers (PDF)

AUTHOR INFORMATION

Corresponding Authors

Jérôme Cornil − *Laboratory for Chemistry of Novel Materials, Center of Innovation and Research in Materials and Polymers (CIRMAP), University of Mons, UMONS, 7000 Mons, Belgium*; orcid.org/0000-0002-5479-4227; Email: jerome.cornil@umons.ac.be

Pascal Gerbaux − *Organic Synthesis and Mass Spectrometry Laboratory, Center of Innovation and Research in Materials and Polymers (CIRMAP), University of Mons, UMONS, 7000 Mons, Belgium*; orcid.org/0000-0001-5114-4352; Email: pascal.gerbaux@umons.ac.be

Authors

Perrine Weber − *Organic Synthesis and Mass Spectrometry Laboratory, Center of Innovation and Research in Materials and Polymers (CIRMAP) and Laboratory of Polymeric and Composite Materials, Center of Innovation and Research in Materials and Polymers (CIRMAP), University of Mons, UMONS, 7000 Mons, Belgium*

Sébastien Hoyas − *Organic Synthesis and Mass Spectrometry Laboratory, Center of Innovation and Research in Materials and Polymers (CIRMAP) and Laboratory for Chemistry of Novel Materials, Center of Innovation and Research in Materials and Polymers (CIRMAP), University of Mons, UMONS, 7000 Mons, Belgium*

Émilie Halin − *Organic Synthesis and Mass Spectrometry Laboratory, Center of Innovation and Research in Materials and Polymers (CIRMAP), University of Mons, UMONS, 7000 Mons, Belgium*

Olivier Coulembier − *Laboratory of Polymeric and Composite Materials, Center of Innovation and Research in Materials and Polymers (CIRMAP), University of Mons, UMONS, 7000 Mons, Belgium*; orcid.org/0000-0001-5753-7851

https://doi.org/10.1021/acs.biomac.1c01442
Biomacromolecules XXXX, XXX, XXX−XXX

Julien De Winter − *Organic Synthesis and Mass Spectrometry Laboratory, Center of Innovation and Research in Materials and Polymers (CIRMAP), University of Mons, UMONS, 7000 Mons, Belgium;* orcid.org/0000-0003-3429-5911

Complete contact information is available at: https://pubs.acs.org/10.1021/acs.biomac.1c01442

Author Contributions

P.W. and E.H have performed the experiments under the supervision of J.D.W., O.C., and P.G and S.H. performed the calculations under the supervision of J.C. All authors have contributed to the writing of the manuscript and given their approval to the final version.

Notes

The authors declare no competing financial interest.

■ ACKNOWLEDGMENTS

The work in the Laboratory for Chemistry of Novel Materials was supported by the Consortium des "Equipements de Calcul Intensif" funded by the Fonds National de la Recherche Scientifique (F.R.S.-FNRS) under grant no. 2.5020.11. The S^2MOs lab is grateful to the FRS-FNRS for financial support in the acquisition of the Waters Synapt G2-S*i* mass spectrometer. J.C., O.C., and P.W. are FNRS research fellows. S.H. thanks the "Fonds pour la Recherche Industrielle et Agricole" for his Ph.D. grant.

■ REFERENCES

(1) Gidden, J.; Bushnell, J. E.; Bowers, M. T. Gas-Phase Conformations and Folding Energetics of Oligonucleotides: DTG $^-$ and DGT $^-$. *J. Am. Chem. Soc.* **2001**, *123*, 5610−5611.

(2) Harvey, S. R.; MacPhee, C. E.; Barran, P. E. Ion Mobility Mass Spectrometry for Peptide Analysis. *Methods* **2011**, *54*, 454−461.

(3) Konijnenberg, A.; Butterer, A.; Sobott, F. Native Ion Mobility-Mass Spectrometry and Related Methods in Structural Biology. *Biochim. Biophys. Acta Protein Proteonomics* **2013**, *1834*, 1239−1256.

(4) Porrini, M.; Rosu, F.; Rabin, C.; Darré, L.; Gómez, H.; Orozco, M.; Gabelica, V. Compaction of Duplex Nucleic Acids upon Native Electrospray Mass Spectrometry. *ACS Cent. Sci.* **2017**, *3*, 454−461.

(5) Boeri Erba, E.; Petosa, C. The Emerging Role of Native Mass Spectrometry in Characterizing the Structure and Dynamics of Macromolecular Complexes: The Emerging Role of Native Mass Spectrometry. *Protein Sci.* **2015**, *24*, 1176−1192.

(6) Barth, M.; Schmidt, C. Native Mass Spectrometry—A Valuable Tool in Structural Biology. *J. Mass Spectrom.* **2020**, *55*, No. e4578.

(7) Hudgins, R. R.; Ratner, M. A.; Jarrold, M. F. Design of Helices That Are Stable in Vacuo. *J. Am. Chem. Soc.* **1998**, *120*, 12974−12975.

(8) Hudgins, R. R.; Mao, Y.; Ratner, M. A.; Jarrold, M. F. Conformations of GlynH+ and AlanH+ Peptides in the Gas Phase. *Biophys. J.* **1999**, *76*, 1591−1597.

(9) Kohtani, M.; Kinnear, B. S.; Jarrold, M. F. Metal-Ion Enhanced Helicity in the Gas Phase. *J. Am. Chem. Soc.* **2000**, *122*, 12377−12378.

(10) Kaleta, D. T.; Jarrold, M. F. Helix−Turn−Helix Motifs in Unsolvated Peptides. *J. Am. Chem. Soc.* **2003**, *125*, 7186−7187.

(11) Kim, D.; Wagner, N.; Wooding, K.; Clemmer, D. E.; Russell, D. H. Ions from Solution to the Gas Phase: A Molecular Dynamics Simulation of the Structural Evolution of Substance P during Desolvation of Charged Nanodroplets Generated by Electrospray Ionization. *J. Am. Chem. Soc.* **2017**, *139*, 2981−2988.

(12) Kondalaji, S. G.; Khakinejad, M.; Valentine, S. J. Comprehensive Peptide Ion Structure Studies Using Ion Mobility Techniques: Part 3. Relating Solution-Phase to Gas-Phase Structures. *J. Am. Soc. Mass Spectrom.* **2018**, *29*, 1665−1677.

(13) Donor, M. T.; Ewing, S. A.; Zenaidee, M. A.; Donald, W. A.; Prell, J. S. Extended Protein Ions Are Formed by the Chain Ejection Model in Chemical Supercharging Electrospray Ionization. *Anal. Chem.* **2017**, *89*, 5107−5114.

(14) Fernandez de la Mora, J. Electrospray Ionization of Large Multiply Charged Species Proceeds via Dole's Charged Residue Mechanism. *Anal. Chim. Acta* **2000**, *406*, 93−104.

(15) DeWinter, J. .; Lemaur, V. .; Ballivian, R. .; Chirot, F. .; Coulembier, O. .; Antoine, R. .; Lemoine, J. .; Cornil, J. .; Dubois, P. .; Dugourd, P. .; Gerbaux, P. . Size Dependence of the Folding of Multiply Charged Sodium Cationized Polylactides Revealed by Ion Mobility Mass Spectrometry and Molecular Modelling. *Chemistry* **2011**, *17*, 9738−9745.

(16) Lanucara, F.; Holman, S. W.; Gray, C. J.; Eyers, C. E. The Power of Ion Mobility-Mass Spectrometry for Structural Characterization and the Study of Conformational Dynamics. *Nat. Chem.* **2014**, *6*, 281−294.

(17) Gabelica, V.; Marklund, E. Fundamentals of Ion Mobility Spectrometry. *Curr. Opin. Chem. Biol.* **2018**, *42*, 51−59.

(18) Gabelica, V.; Shvartsburg, A. A.; Afonso, C.; Barran, P.; Benesch, J. L. P.; Bleiholder, C.; Bowers, M. T.; Bilbao, A.; Bush, M. F.; Campbell, J. L.; Campuzano, I. D. G.; Causon, T.; Clowers, B. H.; Creaser, C. S.; De Pauw, E.; Far, J.; Fernandez-Lima, F.; Fjeldsted, J. C.; Giles, K.; Groessl, M.; Hogan, C. J.; Hann, S.; Kim, H. I.; Kurulugama, R. T.; May, J. C.; McLean, J. A.; Pagel, K.; Richardson, K.; Ridgeway, M. E.; Rosu, F.; Sobott, F.; Thalassinos, K.; Valentine, S. J.; Wyttenbach, T. Recommendations for Reporting Ion Mobility Mass Spectrometry Measurements. *Mass Spectrom. Rev.* **2019**, *38*, 291−320.

(19) Marklund, E. G.; Degiacomi, M. T.; Robinson, C. V.; Baldwin, A. J.; Benesch, J. L. P. Collision Cross Sections for Structural Proteomics. *Structure* **2015**, *23*, 791−799.

(20) D'Atri, V.; Porrini, M.; Rosu, F.; Gabelica, V. Linking Molecular Models with Ion Mobility Experiments. Illustration with a Rigid Nucleic Acid Structure: Ion Mobility Calculations and Experiments. *J. Mass Spectrom.* **2015**, *50*, 711−726.

(21) Albrieux, F.; Calvo, F.; Chirot, F.; Vorobyev, A.; Tsybin, Y. O.; Lepère, V.; Antoine, R.; Lemoine, J.; Dugourd, P. Conformation of Polyalanine and Polyglycine Dications in the Gas Phase: Insight from Ion Mobility Spectrometry and Replica-Exchange Molecular Dynamics. *J. Phys. Chem. A* **2010**, *114*, 6888−6896.

(22) Gelb, A. S.; Lai, R.; Li, H.; Dodds, E. D. Composition and Charge State Influence on the Ion-Neutral Collision Cross Sections of Protonated N-Linked Glycopeptides: An Experimental and Theoretical Deconstruction of Coulombic Repulsion *vs.* Charge Solvation Effects. *Analyst* **2019**, *144*, 5738−5747.

(23) Hoyas, S.; Halin, E.; Lemaur, V.; De Winter, J.; Gerbaux, P.; Cornil, J. Helicity of Peptoid Ions in the Gas Phase. *Biomacromolecules* **2020**, *21*, 903−909.

(24) Duez, Q.; Metwally, H.; Hoyas, S.; Lemaur, V.; Cornil, J.; De Winter, J.; Konermann, L.; Gerbaux, P. Effects of Electrospray Mechanisms and Structural Relaxation on Polylactide Ion Conformations in the Gas Phase: Insights from Ion Mobility Spectrometry and Molecular Dynamics Simulations. *Phys. Chem. Chem. Phys.* **2020**, *22*, 4193−4204.

(25) Zuckermann, R.; Kerr, J.; Kent, S.; Moos, W. Efficient Method for the Preparation of Peptoids [Oligo(N-Substituted Glycines)]. *J. Am. Chem. Soc.* **1992**, *114*, 10646−10647.

(26) Zuckermann, R. N.; Martin, E. J.; Spellmeyer, D. C.; Stauber, G. B.; Shoemaker, K. R.; Kerr, J. M.; Figliozzi, G. M.; Goff, D. A.; Siani, M. A.; Simon, R. J.; Banville, S. C.; Brown, E. G.; Wang, L.; Richter, L. S.; Moos, W. H. Discovery of Nanomolar Ligands for 7-Transmembrane G-Protein-Coupled Receptors from a Diverse N-(Substituted)Glycine Peptoid Library. *J. Med. Chem.* **1994**, *37*, 2678−2685.

(27) Lin, H.; Yan, T.; Wang, L.; Guo, F.; Ning, G.; Xiong, M. Statistical Design, Structural Analysis, and in Vitro Susceptibility Assay of Antimicrobial Peptoids to Combat Bacterial Infections. *J. Chemom.* **2016**, *30*, 369−376.

(28) Maayan, G.; Ward, M. D.; Kirshenbaum, K. Folded Biomimetic Oligomers for Enantioselective Catalysis. *Proc. Natl. Acad. Sci. U.S.A.* **2009**, *106*, 13679−13684.
(29) Kang, B.; Yang, W.; Lee, S.; Mukherjee, S.; Forstater, J.; Kim, H.; Goh, B.; Kim, T.-Y.; Voelz, V. A.; Pang, Y.; Seo, J. Precisely Tuneable Energy Transfer System Using Peptoid Helix-Based Molecular Scaffold. *Sci. Rep.* **2017**, *7*, 4786.
(30) Mahmoudi, N.; Reed, L.; Moix, A.; Alshammari, N.; Hestekin, J.; Servoss, S. L. PEG-Mimetic Peptoid Reduces Protein Fouling of Polysulfone Hollow Fibers. *Colloids Surf., B* **2017**, *149*, 23−29.
(31) Armand, P.; Kirshenbaum, K.; Goldsmith, R. A.; Farr-Jones, S.; Barron, A. E.; Truong, K. T. V.; Dill, K. A.; Mierke, D. F.; Cohen, F. E.; Zuckermann, R. N.; Bradley, E. K. NMR Determination of the Major Solution Conformation of a Peptoid Pentamer with Chiral Side Chains. *Proc. Natl. Acad. Sci. U.S.A.* **1998**, *95*, 4309−4314.
(32) Huang, K.; Wu, C. W.; Sanborn, T. J.; Patch, J. A.; Kirshenbaum, K.; Zuckermann, R. N.; Barron, A. E.; Radhakrishnan, I. A Threaded Loop Conformation Adopted by a Family of Peptoid Nonamers. *J. Am. Chem. Soc.* **2006**, *128*, 1733−1738.
(33) Yoo, B.; Kirshenbaum, K. Peptoid Architectures: Elaboration, Actuation, and Application. *Curr. Opin. Chem. Biol.* **2008**, *12*, 714−721.
(34) Crapster, J. A.; Guzei, I. A.; Blackwell, H. E. A Peptoid Ribbon Secondary Structure. *Angew. Chem., Int. Ed.* **2013**, *52*, 5079−5084.
(35) Gorske, B. C.; Mumford, E. M.; Gerrity, C. G.; Ko, I. A Peptoid Square Helix via Synergistic Control of Backbone Dihedral Angles. *J. Am. Chem. Soc.* **2017**, *139*, 8070−8073.
(36) Morimoto, J.; Fukuda, Y.; Kuroda, D.; Watanabe, T.; Yoshida, F.; Asada, M.; Nakamura, T.; Senoo, A.; Nagatoishi, S.; Tsumoto, K.; Sando, S. A Peptoid with Extended Shape in Water. *J. Am. Chem. Soc.* **2019**, *141*, 14612−14623.
(37) Miller, S. M.; Simon, R. J.; Ng, S.; Zuckermann, R. N.; Kerr, J. M.; Moos, W. H. Proteolytic Studies of Homologous Peptide and N-Substituted Glycine Peptoid Oligomers. *Bioorg. Med. Chem. Lett.* **1994**, *4*, 2657−2662.
(38) Sanborn, T. J.; Wu, C. W.; Zuckermann, R. N.; Barron, A. E. Extreme Stability of Helices Formed by Water-Soluble Poly-N-Substituted Glycines (Polypeptoids) with α-Chiral Side Chains. *Biopolymers* **2002**, *63*, 12−20.
(39) Hara, T.; Durell, S. R.; Myers, M. C.; Appella, D. H. Probing the Structural Requirements of Peptoids That Inhibit HDM2−p53 Interactions. *J. Am. Chem. Soc.* **2006**, *128*, 1995−2004.
(40) Sun, J.; Li, Z. 7 - Peptoid Applications in Biomedicine and Nanotechnology. In *Peptide Applications in Biomedicine, Biotechnology and Bioengineering*; Koutsopoulos, S., Ed.; Woodhead Publishing, 2018; pp 183−213.
(41) Wu, C. W.; Sanborn, T. J.; Huang, K.; Zuckermann, R. N.; Barron, A. E. Peptoid Oligomers with α-Chiral, Aromatic Side Chains: Sequence Requirements for the Formation of Stable Peptoid Helices. *J. Am. Chem. Soc.* **2001**, *123*, 6778−6784.
(42) Armand, P.; Kirshenbaum, K.; Falicov, A.; Dunbrack, R. L.; Dill, K. A.; Zuckermann, R. N.; Cohen, F. E. Chiral N-Substituted Glycines Can Form Stable Helical Conformations. *Fold Des.* **1997**, *2*, 369−375.
(43) Hoyas, S.; Weber, P.; Halin, E.; Coulembier, O.; De Winter, J.; Cornil, J.; Gerbaux, P. Helical Peptoid Ions in the Gas Phase: Thwarting the Charge Solvation Effect by H-Bond Compensation. *Biomacromolecules* **2021**, *22*, 3543−3551.
(44) Haeffner, F.; Merle, J. K.; Irikura, K. K. N-Protonated Isomers as Gateways to Peptide Ion Fragmentation. *J. Am. Soc. Mass Spectrom.* **2011**, *22*, 2222−2231.
(45) Hudgins, R. R.; Jarrold, M. F. Helix Formation in Unsolvated Alanine-Based Peptides: Helical Monomers and Helical Dimers. *J. Am. Chem. Soc.* **1999**, *121*, 3494−3501.
(46) Spencer, R. K.; Butterfoss, G. L.; Edison, J. R.; Eastwood, J. R.; Whitelam, S.; Kirshenbaum, K.; Zuckermann, R. N. Stereochemistry of Polypeptoid Chain Configurations. *Biopolymers* **2019**, *110*, No. e23266.
(47) Frisch, M. J.; Trucks, G. W.; Schlegel, H. B.; Scuseria, G. E.; Robb, M. A.; Cheeseman, J. R.; Scalmani, G.; Barone, V.; Petersson, G. A.; Nakatsuji, H.; Li, X.; Caricato, M.; Marenich, A. V.; Bloino, J.; Janesko, B. G.; Gomperts, R.; Mennucci, B.; Hratchian, H. P. *Gaussian 16*; Gaussian, Inc, 2016.
(48) Grimme, S.; Antony, J.; Ehrlich, S.; Krieg, H. A Consistent and Accurate Ab Initio Parametrization of Density Functional Dispersion Correction (DFT-D) for the 94 Elements H-Pu. *J. Chem. Phys.* **2010**, *132*, 154104.
(49) Ewing, S. A.; Donor, M. T.; Wilson, J. W.; Prell, J. S. Collidoscope: An Improved Tool for Computing Collisional Cross-Sections with the Trajectory Method. *J. Am. Soc. Mass Spectrom.* **2017**, *28*, 587−596.
(50) Allen, S. J.; Giles, K.; Gilbert, T.; Bush, M. F. Ion Mobility Mass Spectrometry of Peptide, Protein, and Protein Complex Ions Using a Radio-Frequency Confining Drift Cell. *Analyst* **2016**, *141*, 884−891.
(51) Ruotolo, B. T.; Benesch, J. L. P.; Sandercock, A. M.; Hyung, S.-J.; Robinson, C. V. Ion Mobility−Mass Spectrometry Analysis of Large Protein Complexes. *Nat. Protoc.* **2008**, *3*, 1139−1152.
(52) Duez, Q.; Josse, T.; Lemaur, V.; Chirot, F.; Choi, C. M.; Dubois, P.; Dugourd, P.; Cornil, J.; Gerbaux, P.; De Winter, J. Correlation between the Shape of the Ion Mobility Signals and the Stepwise Folding Process of Polylactide Ions: Stepwise Folding Process of Polylactide Ions. *J. Mass Spectrom.* **2017**, *52*, 133−138.
(53) Poyer, S.; Comby-Zerbino, C.; Choi, C. M.; MacAleese, L.; Deo, C.; Bogliotti, N.; Xie, J.; Salpin, J.-Y.; Dugourd, P.; Chirot, F. Conformational Dynamics in Ion Mobility Data. *Anal. Chem.* **2017**, *89*, 4230−4237.
(54) Duez, Q.; Liénard, R.; Moins, S.; Lemaur, V.; Coulembier, O.; Cornil, J.; Gerbaux, P.; De Winter, J. One Step Further in the Characterization of Synthetic Polymers by Ion Mobility Mass Spectrometry: Evaluating the Contribution of End-Groups. *Polymers* **2019**, *11*, 688.
(55) Haler, J. R. N.; Morsa, D.; Lecomte, P.; Jérôme, C.; Far, J.; De Pauw, E. Predicting Ion Mobility-Mass Spectrometry Trends of Polymers Using the Concept of Apparent Densities. *Methods* **2018**, *144*, 125−133.
(56) Kokubo, S.; Vana, P. Obtaining the Dielectric Constant of Polymers from Doubly Charged Species in Ion-Mobility Mass Spectrometry. *Macromol. Chem. Phys.* **2017**, *218*, 1700126.
(57) Saintmont, F.; De Winter, J.; Chirot, F.; Halin, E.; Dugourd, P.; Brocorens, P.; Gerbaux, P. How Spherical Are Gaseous Low Charged Dendrimer Ions: A Molecular Dynamics/Ion Mobility Study? *J. Am. Soc. Mass Spectrom.* **2020**, *31*, 1673−1683.

https://doi.org/10.1021/acs.biomac.1c01442
Biomacromolecules XXXX, XXX, XXX−XXX